



Modeling of wave-induced irradiance variability in the upper ocean mixed layer

M. Hieronymi^{1,2}, A. Macke², and O. Zielinski³

¹Helmholtz Centre for Ocean Research, GEOMAR, Kiel, Germany

²Leibniz Institute for Tropospheric Research, IFT, Leipzig, Germany

³Institute for Chemistry and Biology of the Marine Environment, ICBM, Oldenburg, Germany

Correspondence to: A. Macke (macke@tropos.de)

Received: 25 August 2011 – Published in Ocean Sci. Discuss.: 24 October 2011

Revised: 10 January 2012 – Accepted: 24 January 2012 – Published: 1 March 2012

Abstract. A Monte Carlo based radiative transfer model has been developed for calculating the availability of solar radiation within the top 100 m of the ocean. The model is optimized for simulations of spatial high resolution downwelling irradiance E_d fluctuations that arise from the lensing effect of waves at the water surface. In a first step the accuracy of simulation results has been verified by measurements of the oceanic underwater light field and through intercomparison with an established radiative transfer model. Secondly the potential depth-impact of nonlinear shaped single waves, from capillary to swell waves, is assessed by considering the most favorable conditions for light focusing, i.e. monochromatic light at 490 nm, very clear oceanic water with a low chlorophyll *a* content of 0.1 mg m^{-3} and high sun elevation. Finally light fields below irregular wave profiles accounting for realistic sea states were simulated. Our simulation results suggest that under open ocean conditions light flashes with 50 % irradiance enhancements can appear down to 35 m depth, and light variability in the range of $\pm 10\%$ compared to the mean E_d is still possible in 100 m depth.

diance affects several processes in the photic zone of the upper ocean, including photosynthesis of marine phytoplankton (e.g. Walsh and Legendre, 1983; Falkowski, 1984; Wozniak et al., 2003; Dickey et al., 2011).

Several experimental studies in the past were devoted to characterize the statistical properties of fluctuations of the underwater radiance and irradiance field. Field measurements show that the fluctuations of downwelling irradiance E_d are at maximum in clear waters, under clear skies, with high sun altitudes, at wavelengths in the blue-green spectral range, and near the surface within the first ten metres (Dera and Gordon, 1968; Snyder and Dera, 1970; Nikolayev and Prokopov, 1977; Dera and Stramski, 1986). The latest radiometric measurements show very intense fluctuations in irradiance (at 532 nm wavelength and at 0.86 m depth) with peaks exceeding the mean irradiance by a factor of 13 (Gernez et al., 2011). The three-dimensional profile of the water surface determines the light variability within the water column. Different kinds of surface waves, from capillary to fully developed ocean waves, generate characteristic spatiotemporal light patterns at corresponding optical depths (e.g. Nikolayev and Yakubenko, 1978b; Fraser et al., 1980; Wijesekera et al., 2005; Hieronymi and Macke, 2010). Thus, the statistical characteristics of the underwater light field correlate with wind and sea state conditions (e.g. Nikolayev and Yakubenko, 1978a; Gernez and Antoine, 2009). According to Dera and Stramski (1986) and Gernez and Antoine (2009), the most effective waves in terms of their lensing efficiency are caused by light winds between 1 and 5 m s^{-1} . But there are uncertainties concerning the effectiveness and influence of ocean waves on the underwater light field, since many of

1 Introduction

The supply of solar energy to the upper ocean is subject to highly erratic fluctuations, e.g. depending on the sun position, the spectral range of radiation, cloud conditions, water properties and the water depth. In addition, very intense fluctuations occur when sunlight is focused and defocused due to the lensing effect of waves on the water surface, which is the subject of this paper. The variability of spectral irra-

the published data sets have been collected relatively close to the coasts, where generally sea states and waves are not fully developed compared to the open ocean. This issue is addressed within this paper.

The impact of a wind-roughened sea surface on the mean conditions of the underwater light regime and the mechanisms of the wave lensing effect have been investigated numerically over a long period. Wind affects the surface albedo (irradiance reflectance) and the in-water transmission angles of incident light (Preisendorfer and Mobley, 1986), which influences the mean downwelling irradiance in the water. This phenomenon is taken into account in classical atmosphere-ocean radiative transfer models, where stochastic wind-depending wave slope distributions by Cox and Munk (1954) are implemented (e.g. Plass et al., 1975; Mobley et al., 1993). Up to now, this description of the rough air-sea interface is generally applied for example in the *HydroLight* software by Mobley (1994) or in the *MOMO* code by Fell and Fischer (2001). The extreme variance of radiative fluxes near the surface due to the lensing effect cannot be adequately simulated with randomly distributed wave slopes. For this task a well-defined wave structure is needed. The focusing effect of simplified single waves, for example, was studied by means of geometric ray tracing by Schenck (1957), Nikolayev and Khulapov (1975), Dera and Stramski (1988), and Zaneveld et al. (2001). The irregular character of the underwater irradiance distribution is taken into account by implementation of random sea surfaces into the models, that are represented as a superposition of elementary waves from a wave spectrum (e.g. Nikolayev et al., 1972; Yakubenko and Nikolayev, 1977; Weber, 2010; You et al., 2010).

Regarding previous modeling works three points should be improved: (1) the description of the sea surfaces should be more realistic, accounting for all spectral ranges of ocean waves; furthermore the actual wave elevations (in z -direction) should be explicitly implemented into the radiative transfer model. (2) The model should allow for scattering and absorption of light within the water column, and (3) the depth resolution of the underwater light field should be significantly enhanced at all relevant water depths. The present work gives an approach for solving these issues. We introduce a novel Monte Carlo (MC) radiative transfer model, which is optimized for fast and spatial high-resolution simulations of the underwater light field below any user-defined shape of the water surface. By means of the model, we show the impact of nonlinear shaped single waves and examples with realistic wave profiles that consist of all wave sizes from capillary to swell waves. The two-dimensional MC model covers a large spatial light field with high resolution and it considers the actual vertical wave deflection. The model is based on homogeneous inherent optical properties (IOPs) of very clear seawater, which is common within the mixed surface layer of the open ocean. Most related publications focus on extreme light fluctuations near the surface down to

10 m water depth only (e.g. You et al., 2010; Gernez et al., 2011). We additionally simulate the availability of downwelling irradiance and its fluctuations down to 100 m depth. Deep-water light fluctuations may be of particular importance for the radiative energy supply for deep chlorophyll a maxima which often develop between 20 and 150 m depth (e.g. Cullen, 1982; Furuya, 1990; Zielinski et al., 2002). Our modeling results for the underwater light field are compared with radiometric measurements from open ocean studies and against the *HydroLight* radiative transfer code, to verify the suitability of our model.

2 Methods

2.1 Field study

Measurements have been carried out in 2009 on board the R/V *Polarstern* during a north-south traverse of the tropical and subtropical Atlantic Ocean (El Nagggar and Macke, 2010). The data sets here presented have been recorded during local noon time under direct sun and nearly clear sky conditions. Downwelling irradiance within the water column was measured with a *Ramses-ACC-VIS* radiometer with a spectral range of 320 to 950 nm (*TriOS*, Germany). E_d spectra were each sampled over a period of 2 min per depth level down to 45 m water depth (sensor integration times between 16 and 128 ms, step sizes in depth 2, 2.5 and 5 m). Thus, we obtained mean values of the light field and indication of the irradiance variance in the water column. Within these upper 45 m, CTD (*SBE 911plus*, *Sea-Bird Electronics*, USA) measurements showed well-mixed and non-stratified seawater with an approximate chlorophyll a content of 0.1 mg m^{-3} ($\pm 0.02 \text{ mg m}^{-3}$). Suspended particles and colored dissolved organic matter (CDOM, also referred to as *Gelbstoff*) not related to the phytoplankton content were negligible. At one station (16 November 2009) we observed a well-pronounced deep chlorophyll maximum located from 60 to 75 m depth (in CTD measurements down to 200 m). Registration of sea states with differentiation of wind-sea and swell has been accomplished by an on-board meteorologist via visual assessment (see Table 1 for details).

In addition to the radiometric measurements, a specially developed underwater camera system was utilized to film areal light patterns that are projected on a white screen at different water depths (not shown here, see Hieronimi and Macke (2010) and Hieronimi (2011) for details and results).

2.2 Model description

Light fluctuations in water originate from the geometrical superposition of individual light beams that are refracted at the wave surface. Depending on the inherent optical properties IOPs of the water body, solar radiation is scattered and absorbed, which leads to a spatial spreading and attenuation of the initial light beam. When modeling the focusing effect of

Table 1. Environmental conditions at three measuring sites onboard the R/V *Polarstern* (cruise ANT-XXVI/1) with same inherent optical properties of the upper ocean mixed layer.

Date		30 October 2009	3 November 2009	16 November 2009
Location		19°44 N 23° W	4°54 N 23° W	32°38 S 41°7 W
Sun zenith angle	[°]	33.7	22.8	15.5
E_d (490 nm) at the surface	[mW m ⁻² nm ⁻¹]	1271	1397	1475
Wind speed	[m s ⁻¹]	11.0	5.4	10.0
Wind sea wave height	[m]	1.5	0.5	2.0
Wind sea wave period	[s]	5.0	3.0	5.0
Swell wave height	[m]	2.0	1.5	1.5
Swell wave period	[s]	9.5	8.5	8.0

Table 2. Inherent optical properties of the considered water body at 490 nm wavelength and with 0.1 mg m⁻³ chlorophyll *a* concentration (Morel et al., 2007; Morel, 2009).

Absorption coefficient (total)	a	[m ⁻¹]	0.0280
– of seawater	a_{sw}	[m ⁻¹]	0.0150
– of particles	a_p	[m ⁻¹]	0.0082
– of CDOM	a_y	[m ⁻¹]	0.0048
Scattering coefficient (total)	b	[m ⁻¹]	0.0793
– of seawater	b_{sw}	[m ⁻¹]	0.0030
– of particles	b_p	[m ⁻¹]	0.0763
Attenuation coefficient (total)	c	[m ⁻¹]	0.1072
– due to particles	c_p	[m ⁻¹]	0.0844

surface waves, light beams and the entire spread pattern must be superposed with respect to a spatial allocation.

The radiative transfer in water is mostly simulated by means of the Monte Carlo method (e.g. Plass et al., 1975; Mobley et al., 1993; Deckert and Michael, 2006; D'Alimonte et al., 2010). The physical processes of scattering, absorption and surface reflection/transmission are simulated for a sufficiently large number of individual photons, which is relatively time-consuming. In our model, time-consuming MC simulations are decoupled from the relatively fast geometric ray tracing for light fluctuation analysis. Once the light beam enters the water body with a specific transmission angle, its propagation is always equal at steady IOPs. By means of our model, it is possible to compute the definite geometric pattern of underwater light fields below arbitrary waves, taking into account all direct and diffuse radiative fractions.

2.2.1 Underlying data and boundary conditions

The model input parameters are selected in such a manner that maximum light field variability can be achieved (Dera and Stramski, 1986; Walker, 1994; Gernez and Antoine,

2009). The radiative transfer simulations are carried out for monochromatic light at a wavelength of 490 nm; in this spectral range the water itself is very transparent for light (Pope and Fry, 1997). The chlorophyll *a* concentration Chl of the entire photic water column is chosen to be 0.1 mg m⁻³, corresponding to very clear and oligotrophic oceanic water that can be found over a wide range of the tropical and subtropical regions of the earth; indeed, the annual mean value of Chl for the deep global ocean amounts to 0.193 mg m⁻³ (Wang et al., 2005). Table 2 specifies the wavelength- and Chl-dependent IOPs of seawater that are taken from Morel et al. (2007) and Morel (2009), following the concept that optical properties in the upper ocean can be derived from the optical properties of seawater itself and from the chlorophyll *a* content. This water is classified as Case 1 (Morel and Prieur, 1977; Gordon and Morel, 1983), whereas Case 2 refers to the water types with optically active particulate and dissolved matter, not corresponding to the phytoplankton concentration. The refractive index n of seawater, which depends on the wavelength, temperature, and salinity, is set to 1.34 (Segelstein, 1981). We utilized *Petzold's* phase function that accounts for both molecular (water) scattering and scattering at average particles (Petzold, 1972). In this phase function, hydrosols and planktonic particles are treated to be undirected; although we must assume that under high sea conditions particles are affected by considerable hydrodynamic accelerations and thus align preferentially in the direction of the fluid flow, which essentially alters the light scattering properties of seawater (Marcos et al., 2011). Another point that is neglected for this study is inelastic *Raman* scattering. Especially for low Chl, *Raman* emissions generally affect the radiance field. Nevertheless, at the relevant spectral band around 490 nm *Raman* scattering plays a minor role only (Morel et al., 2002). Scattering is regarded as perfectly elastic and polarization effects are not considered. Furthermore, neither whitecaps nor bubbles near the surface are regarded in the model. Both can have strong effects on light scattering at the air-water interface and within the upper water layer, their influence starting at moderate winds (about 5 m s⁻¹) and further rising with increasing wind (Stramski and Tegowski,

Table 3. Classification of the single wave types with details for corresponding model domains.

Wave class		1	2	3	4	5
Description of wave class		Small Ultra Gravity	Medium Ultra Gravity	Large Ultra Gravity	Ordinary Gravity	Ocean Waves
Wave length	L [m]	0.025–0.1	0.15–0.5	0.6–1.4	1.5–20	25–192
Wave period	T [s]	0.12–0.26	0.31–0.57	0.6–1.0	1.0–3.6	4–11
Wave height	H [m]	0.0008–0.009	0.0045–0.045	0.018–0.126	0.045–1.8	0.5–7.5
Wave steepness	H/L [–]	0.03, 0.06, 0.09	0.03, 0.06, 0.09	0.03, 0.06, 0.09	0.03, 0.06, 0.09	0.002–0.13
Applied Method		Ray tracing	Ray tracing	Monte Carlo	Monte Carlo	Monte Carlo
Grid depth	z [m]	2	5	10	40	100
Grid width	x [m]	–	–	5	20	100
Vertical resolution	dz [m]	0.001	0.001	0.01	0.05	0.1
Detector width	dx [m]	0.0025	0.0025	0.005	0.01	0.1

2001; Zhang et al., 2006). Ignoring whitecaps, bubbles and also flow-induced preferred particle orientation is therefore expected to overestimate the intensity of light focusing under many natural conditions. But for the sake of model simplicity and a better intercomparison of the impact of different wind and wave regimes, we stick to these idealized conditions and note that the largest light variability discussed here should be regarded as an extreme.

2.2.2 The sea surface

Ocean surface waves are assumed to be long-crested waves. They are nearly two-dimensional and the crests appear very long in comparison to the wavelength. Because of this fact and because we are interested in large-scale and high-resolution light fields beneath several hundred metre long wave trains and water depths down to 100 m, we limit the radiative transfer model to a 2-D domain with a two-dimensional description of the wavy surface. The 3-D effect might be of more relevance for simulations of irradiance fluctuations near the surface, where small-scale waves govern the variability (Nikolayev and Yakubenko, 1978b; Hieronymi and Macke, 2010). Such 3-D simulations are shown by You et al. (2010), where the size of the water surface patch was 2 m \times 2 m with depths under consideration of less than 3 m.

The sea surface consists of a superposition of various waves with different size, orientation and origin. The corresponding subsurface irradiance field is subject to interferences of the single lensing systems, which disable the development of a clear and homogeneous irradiance pattern. In order to understand the principal structure of light fluctuations down the water column we first look at regular single waves and later at irregular wave trains.

In general, most wind-generated gravity waves have a steepness (wave height to length H/L) of about 0.03 to 0.06. In rare events, the wave steepness exceeds 0.09 (theoretically up to 0.14 for deepwater); steeper waves break. The exact shape of the wave has a strong impact on the resulting

light field. Up to now, sinusoidal waves were implemented in radiative transfer models to show the lensing effect of single waves (Schenck, 1957; Dera and Gordon, 1968; Nikolayev and Khulapov, 1976; Stramski and Dera, 1988; Zaneveld et al., 2001; Deckert and Michael, 2006; D'Alimonte et al., 2010). In fact, water waves can be described as sine curves for small amplitudes with H/L of less than 0.006. Steeper waves should be represented by means of *Stokes* wave theory of higher order. Substantial deviations occur in the shape, i.e. the wave crest is higher and sharper and the trough is flattened, and in the hydrodynamical behavior, e.g. the *Stokes* wave moves slightly faster than a small-amplitude wave. Based on the formulation of Kinsman (1965), the non-linear elevation ζ of any gravity wave can be sufficiently described by means of Stokes theory of fourth order:

$$\zeta = \zeta_a \cos kx + \frac{1}{2} k \zeta_a^2 \left(1 + \frac{17}{12} k^2 \zeta_a^2 \right) \cos 2kx + \frac{3}{8} k^2 \zeta_a^3 \cos 3kx + \frac{1}{3} k^3 \zeta_a^4 \cos 4kx, \quad (1)$$

where ζ_a is the amplitude, k the wave number, and kx the phase. The term $k\zeta_a$ stands for the wave steepness, too. The time rate of change of the spatial subsurface light field directly corresponds to the phase speed of the surface wave. Long water waves propagate faster than shorter ones (dispersion). In the first order approximation the water wavelength L and the wave period T are related by:

$$L = \frac{g}{2\pi} T^2, \quad (2)$$

in which g is the acceleration of gravity (*Airy* theory for deepwater gravity waves).

The single waves under consideration are classified into five categories each with size adapted model grid dimensions (for details see Table 3). The smallest realized horizontal grid resolution dx is 2.5 mm, which corresponds to the diameter of fast irradiance sensors (Darecki et al., 2011); the sensor head diameter of the *Ramses-ACC-VIS* is 5 mm. Capillary ($L <$

1.73 cm) and ultra-gravity waves with periods T of less than 1 s are directly associated with local winds. In particular, capillary and small ultra-gravity (also referred to as gravity-capillary) waves in the wavelength range of 0.7 to 3 cm are most dependent on the wind speed (Jähne and Riemer, 1990). Wave classes four and five contain fully developed gravity waves that also arise from wind, but they are not necessarily associated with the local wind situation as waves propagate away from their area of origin. Wind waves with periods of more than 10 s are usually referred to as swell, although also wave systems with periods > 6 s are often called swell, if they are the aftereffect of a previous or distant wind field. Single waves with periods up to 11 s are considered, larger waves are irrelevant in terms of light field fluctuations. According to the ocean wave statistics by Hogben and Lumb (1967), 95 % of all visually observed sea conditions in the tropics and still more than 90 % globally (for all seasons, all directions, and all areas) are accumulated within wave category five.

A natural sea surface is described by the superposition of weighted harmonics from the energy density spectrum of the sea state. In terms of underwater light field modeling, the basic concept was already applied for example by Snyder and Dera (1970), Nikolayev et al. (1972), Yakubenko and Nikolayev (1977), Walker (1994), and You et al. (2010). We used sea wave spectra, where the long wave part (swell and wind-sea) were handled with a double-peaked spectrum according to Ochi and Hubble (1976), and where the short directly wind-driven waves are represented by means of the formulation by Elfouhaily et al. (1997). The input parameters for the wave spectra, consisting of wind speed, wave height and period of wind-sea and swell respectively, are given in Table 1. The resulting unidirectional irregular wave field has a *Gaussian* slope distribution with the same wind-dependent range of wave slopes as observed by Cox and Munk (1954). We do not consider small-scale surface irregularities, such as the short (capillary or gravity-capillary) waves that ride ahead of crests of longer gravity waves (e.g. Longuet-Higgins, 1963) with the subsequent skewness of the *Cox-Munk* slope distribution (Longuet-Higgins, 1982). Nevertheless, in the model all waves are represented with a horizontal resolution dx of 0.1 mm. The irregular water wave profiles are 500 m long and feature all wave characteristics from the applied spectrum, including the especially pronounced gravity-capillary waves at approximately 1.7 cm wavelength (peak of the short wave spectrum) whose steepness depend on the local wind (Elfouhaily et al., 1997).

At the open sea, vertical deflections of the sea surface can be large, e.g. the statistically expected maximum wave height of the observed sea states (Table 1, 30 October 2009) is almost 5 m. However, most comparable models do not account for vertical wave deflections, i.e. the wave structure is regarded as chain of successive wave slopes located at the mean waterline (e.g. Deckert and Michael, 2006; Weber, 2010; You et al., 2010). Nevertheless, surface elevations themselves may act as direct source of light fluctuations.

D'Alimonte et al. (2010) showed a first MC model where the corresponding wave amplitude itself is considered. In our model, the z -variant wave deflection is taken into account.

When the mixing of the upper ocean due to heating and cooling is less important than that due to the waves, then the ocean's mixed layer depth (MLD), can be predicted directly from the significant wave height H_S (defined as the mean height of the one third highest waves) and the peak period T_P of the wave spectrum (Babanin, 2006). Even swell waves have been suggested as a possible source of ocean mixing (Kantha, 2006). In the given examples (Table 1), the calculated wave-induced turbulence reaches down to around 50–60 m depth, which fits to the CTD observations. In case of more pronounced sea states (especially higher waves), the wave-induced MLD can be more than 100 m (Babanin, 2006). With regard to the bio-optical properties of this mixed layer, the depth at which the photosynthetic available radiation *PAR* is reduced to 1 % of its value at the surface (euphotic layer depth) is about 100 m, assuming a uniform chlorophyll *a* concentration of 0.1 mg m^{-3} (Morel, 1988). For this reason, we show wave-caused light field variability down to 100 m water depth. But one should keep in mind that bio-optical and physical properties of the sea strongly vary with season and region (e.g. Dickey et al., 1993; de Boyer Montegut et al., 2004).

2.2.3 Radiative transfer model

Two different model approaches are chosen to deal with the variety of dimension requirements, a Monte Carlo-based model for large-scale irradiance simulations and a simplified ray tracing model for small-scale near-surface conditions. Table 3 gives an overview about the utilized grid sizes and resolutions with respect to the applied methods. The resolution specifications apply accordingly to simulations of irregular wave fields (Sect. 3.3). The basic difference is that the MC-based method considers all direct and diffuse radiation in the water, while the alternative ray tracing model considers the direct light beam only.

Monte Carlo model

The MC procedure that we employ differs in some aspects from other models that have been recently in use (Deckert and Michael, 2006; D'Alimonte et al., 2010; You et al., 2010). There is neither distinction between absorption and scattering as in Kirk (1981), nor a further identification whether the scattering process is caused by water-molecular or particle scattering (Morel and Gentili, 1991). We do not apply the usual concept of photon weight reduction, where the statistical losses by absorption and scattering are assessed by means of the single scattering albedo $\omega_0 = b/c$ (at the scattering position: $w_{\text{new}} = w_{\text{old}} \omega_0$). Instead, in our model the photon path length is determined by the scattering

coefficient b only, and not by the attenuation coefficient c , and the light is continuously attenuated along the propagation path, which only depends on the total absorption coefficient a . Numerically both concepts should give the same results. However, our approach provides a faster convergence of the irradiance pattern since each horizontal grid segment is used as an irradiance detector (e.g. in the 100 m wide \times 100 m deep grid, we have 1000 \times 1000 detectors). Our MC model simulates the radiative transfer inside the water body only. The model domain covers up to 100 m water depth and 100 m width, with light beam access at one single point at the top. In detail the model pursues the following procedure.

If we assume uniform IOPs of the entire water body, then a light beam which enters the surface at a single point should propagate at first always similarly, only depending on its initial in-water transmission angle and its intensity at the surface. The photon tracing starts directly below the surface (at the point [0 0]), whereat all photons have the same initial angle that depends on the insolation angle and the slope of the discrete wave segment and that is determined by *Snell's* law.

The free path length l_S between two subsequent scattering events is determined by the selection of an equally distributed random number R between 0 and 1 and the total scattering coefficient b (Table 2) (Macke, 2000)

$$l_S = -\frac{1}{b} \log(R). \quad (3)$$

With the given IOPs parameterized by $\text{Chl} = 0.1 \text{ mg m}^{-3}$, the mean scattering path length l_S is 12.6 m.

At the scattering point, the light beam changes its propagating direction in accordance to the global scattering phase function β_{p+w} (Morel et al., 2002), where particle (Petzold, 1972) and molecular (*Rayleigh*) scattering are considered. This is numerically implemented using the cumulative scattering distribution

$$D(\psi) = 2\pi \int_0^{2\pi} \beta_{p+w}(\psi) \sin(\psi) d\psi, \quad (4)$$

where a random number between 0 and 1 defines the scattering angle ψ . In natural particle-containing waters, light is predominantly scattered into the forward direction.

The actual attenuation of light occurs along its distance covered, on the grounds that the light beam transits toward a scattering point through an absorbing medium. In our model this approach is realized by a continuous intensity reduction of the light beam characterized by the medium's absorption properties. The intensity of the light beam decays exponentially along the path

$$I = I_0 \exp(-a l_z), \quad (5)$$

with the initial intensity I_0 just after entering the water, the total absorption coefficient a (Table 2), and the total so far covered distance l_z with respect to the depth level z .

Within the water body, light can be scattered back to the water surface. At the water-to-air boundary, which is assumed to be flat here, partial and total reflection occur. According to *Snell's* law total internal reflection happens at nadir angles $\theta > 48^\circ$ (at 490 nm). In this case the photon remains in the system, otherwise a new photon is selected. Partial internal reflection is neglected, as it plays a minor role only (Mobley, 1994). Light can additionally leave the system at all other external grid boundaries (e.g. lateral ± 50 m and at 100 m depth), but never enter again. The model does not allow for periodic boundary conditions as this would violate the concept of the spatial irradiance pattern of a single beam. This is in contrast to other models where periodicity is intended, e.g. D'Alimonte et al. (2010). The model domain, in which the Monte Carlo calculations for a single beam irradiance pattern are conducted, has to be large enough to ensure that the horizontal losses due to domain-leaving photons are negligible. With the given model input values (Table 2), these losses at the side amount to less than 0.01 % of the total downwelling irradiance per water depth compared to a model domain with 200 m width. The model size requirements and the conceptual error of our model concerning the downward scattering from the underside of the wave modulated sea surface are discussed in Hieronimi (2011).

The ray tracing procedure considers a maximum number of scattering events, N_{\max} . As long as the "photon package" does not leave the model domain, its way through the medium is traced up to this number. If the photon leaves the area, a new photon is selected. With the given IOPs (Table 2), N_{\max} is selected to be 40; after travelling more than 500 m ($N_{\max} \cdot l_S$) through the water body on average the "light beam" does not contribute an important intensity anymore (Eq. 5). This approach is consistent with the weight threshold value of 10^{-6} which is often used (e.g. in Plass and Kattawar, 1972; Mobley, 1994; D'Alimonte et al., 2010).

The covered path of the light is known with respect to global coordinates. Thus, the intensity values can be allocated and summed up for each horizontal segment x at a level z . Since the orientation of photon propagation is also known, it can be stated whether its energy contributes to down- or upwelling irradiances, respectively. In the end, the accumulated weights for each grid cell are normalized by the total number of photons that have entered the system. The outputs of the MC model are areal distributions of normalized fractions of down- and upward directed irradiances (E_{dxz} and E_{uxz}). If we add all gridded irradiances at a particular depth, we gain the total amount of diffuse (scattered) and direct (unscattered) irradiance at this depth. This value must be equal to the mean planar downward/upward irradiance (\bar{E}_d and \bar{E}_u , respectively) at this particular depth.

The basic idea of the introduced concept is to decouple the time-consuming MC simulations from relatively fast, geometric super-positioning of spatial light fields that arise from a deflected sea surface. In order to achieve this, we carried out MC simulations for different ray tracing starting angles

between 0° and 70° (downward directed) with an angular spacing of 0.05° to 1° , each with 2×10^5 photons. The corresponding grid size specifications depend on the considered wave size and are given in Table 3 (wave class 3 to 5). All 2-D irradiance grids that result from a single beam photon entry are stored in a database, which then provides a basis for the wave focusing analysis.

Diffuse sky radiation

The total irradiation that enters the water accounts for the direct solar radiation (with zenith angle) and diffuse skylight from atmospheric *Rayleigh* and *Mie* scattering. The fraction of diffuse irradiation depends (amongst other things) on the wavelength, the sun position, cloudiness, and aerosol load (Walker, 1994). For example, an overcast sky with no visible sun is completely diffuse, whereas the ratio of background sky irradiance to total irradiance can be approximately 10% under very clear sky conditions with a high sun elevation at 490 nm wavelength. The distribution of incident angles and the amount of the sky radiance can be computed for example with the model by Zibordi and Voss (1989). In case of a clear sunny atmosphere, the angular distribution of atmospheric diffuse light is close to isotropic (same assumption as in You et al., 2010 and D'Alimonte et al., 2010).

Based on the database with E_{dxz} fields of single beams, the following points are considered to generate a wave slope-dependent E_{dxz} field for diffuse skylight: (1) the incidence of diffuse radiation is assumed to be isotropic. (2) the half-space above the surface is partly shadowed in case of an inclined wave segment. (3) the effective transmission angle of each irradiation part is determined via *Snell's* law, and (4) the transmission rate of each single portion is calculated from *Fresnel's* equations.

Figure 1 shows the downwelling irradiance field for clear sky conditions with 10% diffuse irradiation and 90% direct sun light from 0° zenith angle. The color scale is set logarithmic to resolve the orders of magnitudes of E_{dxz} . The distribution shows a well-defined light cone of about 96° width that is due to the diffuse irradiation and which is associated with *Snell's* window. Nevertheless, most radiative parts are located near to the initial path of the direct sun, e.g. 50% of the total distributed irradiance in the field is accumulated within the 1 m wide water column at $x = 0$.

Superposition of individual light fields

The underwater light field considers all direct and diffuse fractions of the downward directed irradiance with respect to the exact point of insolation at the surface. To compute this, we firstly initialize an overall grid system (with global coordinates x and z) and dimensions of the area of interest, e.g. in case of irregular wave profiles, the field is 500 m wide and more than 100 m deep with a discretization of 0.1 m in

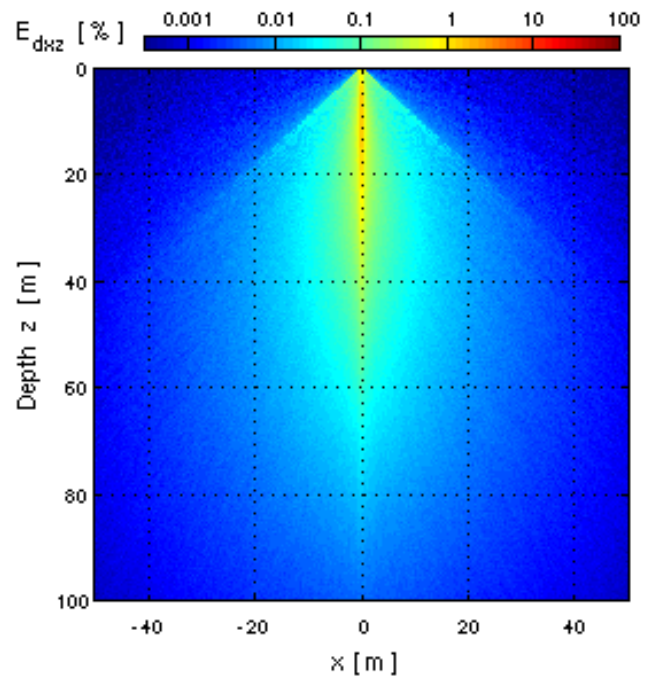


Fig. 1. Spatial expansion of light, in terms of the downwelling irradiance E_d , within the water column due to 90% direct solar irradiation (zenith angle 0°), 10% isotropic diffuse skylight and a non-tilted wave facet (logarithmic color scale).

each direction. Then, the 500 m long wave profile has to be located in the global grid. Now, for each horizontal wave segment a vertical position of light incidence with corresponding wave slope can be allocated. In the next step the global in-water transmission angles and rates are determined via *Snell's* law and the *Fresnel* equations using the relative sun position and the wave slope. Now the total light incidence per 10 cm grid segment at the surface has to be determined. Here, for every wave facet of 0.1 mm width the corresponding 100 m \times 100 m E_{dxz} fields for the single beam and for the diffuse skylight are taken from the database and weighted according to the transmission rate and the ratio of direct-to-diffuse insolation. The complete 100 m \times 100 m field that arises from a 10 cm wide light incidence at the surface must now be adapted to the global coordinate system by taking into account the current surface deflection. Overlapping parts of the individual light fields above the water surface are cut off and are not further considered, just as internal reflections that would occur at a wave-shaped surface; now internal reflection is treated as it would be at a flat surface. Both aspects cause negligibly small errors in the determination of the underwater light field only (Hieronimi, 2011).

The statistical evaluation of the subsurface E_{dxz} field refers to the 400 m wide area in the center only, which includes all diffuse radiation that was inserted within the 500 m wave profile. The vertical length of the water column between the actual surface elevation and a detector is defined

as reference or true depth z_t . In the following all radiative data refer to this reference depth, so that the depth contours (of same hydrostatic pressure) are always shaped as the water surface. The reference depth is handled differently in other publications e.g. in D'Alimonte et al. (2010). The authors refer to a depth displaying the surface wave effects on the pressure gauge and therefore to virtual isobars. This approach makes sense but it is based on linear wave theory, which makes an adaptation onto nonlinear wave systems intricate.

In the discussed case with an irregular wave, we effectively consider 2×10^5 photons per 0.1 mm wave segment over a range of 500 m; this amounts to a total of 10^{12} (one trillion) photons. Sensitivity studies have shown that larger numbers of photons do not yield significantly different results.

Light fluctuations are characterized by parameters, which are normally based on temporal changes of the light field, i.e. measured time series of E_d . This work considers spatial differences. This essentially is the same since both quantities are related by the dispersion equation Eq. (2). The horizontal averaging of all E_{dxz} values at a depth z_t is equal to the total downwelling irradiance \bar{E}_d , which always decreases exponentially with water depth. E_d fluctuations are commonly described by the coefficient of variation

$$CV = \frac{\sigma_E}{\bar{E}_d}, \quad (6)$$

given as the ratio of the standard deviation σ_E and the mean downwelling irradiance at the reference depth. E_d time series are typically normalized, in order to evaluate extreme values and the distribution of occurrence probability (You et al., 2010; Gernez et al., 2011). The normalized downwelling irradiance, in relation to spatial E_d variability, is denoted as

$$\chi = \frac{E_{dxz}}{\bar{E}_d}. \quad (7)$$

It basically describes the multiple of an E_{dxz} value compared to the mean irradiance at a depth. Dera and Stramski (1986) defined irradiance pulses that exceed the mean irradiance by a factor (here χ) of more than 1.5 as underwater light flashes.

Alternative ray tracing model

The top 10 m of the water column are of particular importance in terms of wave-induced light fluctuations, since here light flashes are generally most pronounced and most frequent. Especially in clear ocean water the fraction of scattered light in the total E_d is small in the first metres compared to the direct light beam. Furthermore, most of the scattered light is located very close to the initial propagation direction, because of the predominance of forward scattering. Under these assumptions it is reasonable to only consider the direct beam and to neglect all scattered light.

The fundamental simplification is the utilization of the ray tracing procedure as for example used in Schenck (1957)

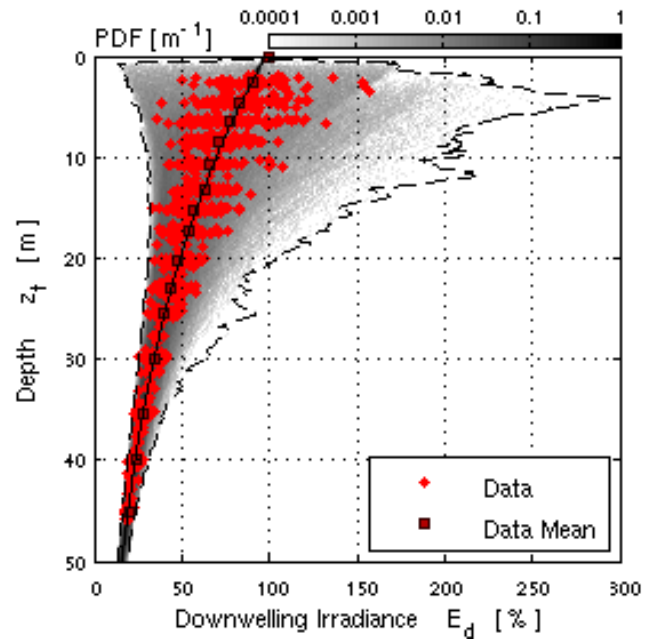


Fig. 2. Comparison of downwelling irradiance E_d as calculated by the model (for 490 nm) vs. offshore measurements with the spectral radiometer at 489 nm (30 October 2009); data points in red with squares for the corresponding mean values, the modeled PDF with $dx = 10$ cm is gray shaded with dashed outlines.

or more recently by Zaneveld et al. (2001) and an additional continuous attenuation of the individual rays by Beer-Lambert's law Eq. (5) (based on the absorption coefficient in our formulation). The contribution of all accumulated rays in a detector field provides an adequate estimate of the downwelling irradiance. Without major accuracy losses, this method is applicable for clear seawater (with the given IOPs) and down to depths of about 5 m (Hieronimi, 2011). This method is computationally more efficient (faster) and allows for high spatial resolution with $dx = 2.5$ mm, i.e. high-frequency analysis.

3 Results and discussion

3.1 Benchmark tests of the model

Model results are compared with data from field measurements (Sect. 2.1) and with the widely used *HydroLight* radiative transfer software by Mobley (1994) using the invariant embedding method. Figure 2 shows one example of measurements (red dots), with corresponding E_d mean values within ± 0.3 m depth range (red squares). The probability density function PDF of simulated E_d is gray shaded with dashed outlines. The solid line represents the total plane downwelling irradiance \bar{E}_d ($dx = 10$ cm model). All measured data are within the range of highest expected occurrence probability; in none of the cases under consideration

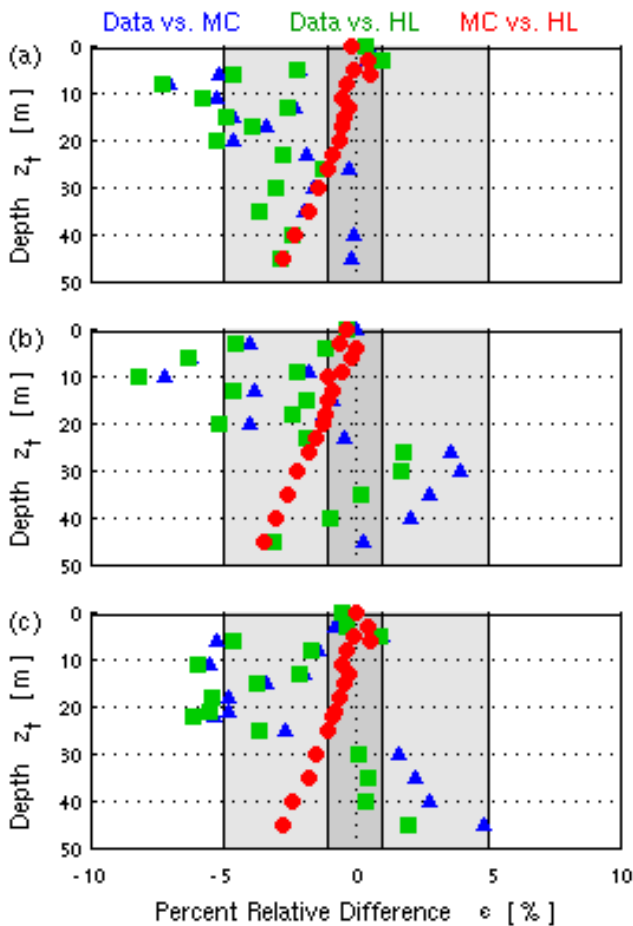


Fig. 3. Percent relative differences of E_d mean values between measured data, our Monte Carlo (MC) model and *HydroLight* (HL); (a) 30 October 2009; (b) 3 November 2009; (c) 16 November 2009, the related conditions are specified in Table 1.

data points lie outside the predicted *PDF* limits. In the shown example, light flashes ($\chi > 1.5$) were registered down to 11 m. The deepest occurrence of light flashes has been observed at 20.8 m depth at another day of the cruise with similar lighting conditions, which is the greatest depth of observed light flash occurrence as far as we know. According to the model, light flashes could be found even in 35 m water depth. Our measurements were not sufficient to show the high-frequency variance that is predicted by the model, the sampling rate and integration time of the used radiometer do not permit high-frequency sampling. However, the high E_d variance near the surface is well documented (e.g. Gernez et al., 2011). The validation of our modeled irradiance distribution, especially at clear seawater, fully developed seas and particularly below the top 10 m layer, is a task for specialized radiometric sensors as the novel system by Darecki et al. (2011).

The mean values of the measured data can be compared to the E_d mean of our Monte Carlo (MC) simulations and

equivalent *HydroLight* (HL) runs with the same wavelength, refractive index of water, sun zenith angle, surface insolation, wind speed, IOPs, scattering phase function, and with the same sky diffuseness. Figure 3 compares the percent relative difference

$$\varepsilon = 100 \frac{\bar{E}_a \bar{E}_b}{\bar{E}_b} \quad (8)$$

of mean values of measured data vs. MC (blue triangles), data vs. HL (green squares), and MC vs. HL (red dots), respectively. The commonly considered uncertainty threshold for in-situ radiometric measurements is 5% (light gray shaded); according to the manufacturer (*TriOS*, Germany) the detection accuracy of our irradiance sensor is better than 6–10% (depending on spectral range). Comparisons of radiative transfer computations result in lower uncertainties, typically within less than 1% (dark gray shaded). Figure 3 shows the comparisons for the three stations whose quite similar environmental conditions are specified in Table 1. Typically the averaging over about 80 data points (2 min each) yields unsteady means, especially in the upper 25 m, where the E_d variance is high. In general, the overall agreement between averaged observations and the modeling results (MC and HL) is satisfying. The agreement between our MC model and *HydroLight* is very good within the top 25 m. Our model tends to overestimate the total light attenuation compared to HL; the bias continuously grows to less than 20% in 100 m depth. These differences, which are still comparable with those of previous model benchmarking (e.g. Mobley et al., 1993; D’Alimonte et al., 2010), can be explained by inherent differences of the applied methods, regarding for example the representation of the diffuse sky light (HL uses an idealized sky model) or the scattering properties of the water (we use a higher interpolated scattering angle discretization, which could affect the scattering pattern and in particular the forward scattering). Another source for deviations is the different sea surface representation. *HydroLight* employs the wind-depending *Cox-Munk* wave slope statistics. Our continuous wave profile accounts for the same local wind conditions but also for a fully developed sea state; its slope distribution resembles a *Cox-Munk* distribution with actually more wind (the *PDF* skewness is not considered). Thus, more light is scattered directly at the rougher surface and \bar{E}_d becomes slightly smaller. Furthermore, the summation of lateral losses of diffuse radiation (beyond the ± 50 m from the photon entry) is another reason for the underestimated total E_d compared to HL especially in greater depths. The lateral losses are small ($< 0.01\%$ per depth) at perpendicular irradiation; a little more escapes at the edges in case of a strongly inclined wave slopes, which occurs more frequently at strong wind. However, by far the most radiation is very close to the direct initial light beam (within ± 10 m), whose direction is determined by the wave slope, even in 100 m depth (see Fig. 1). It is primarily the narrow light beam that causes the reported irradiance variability at depths.

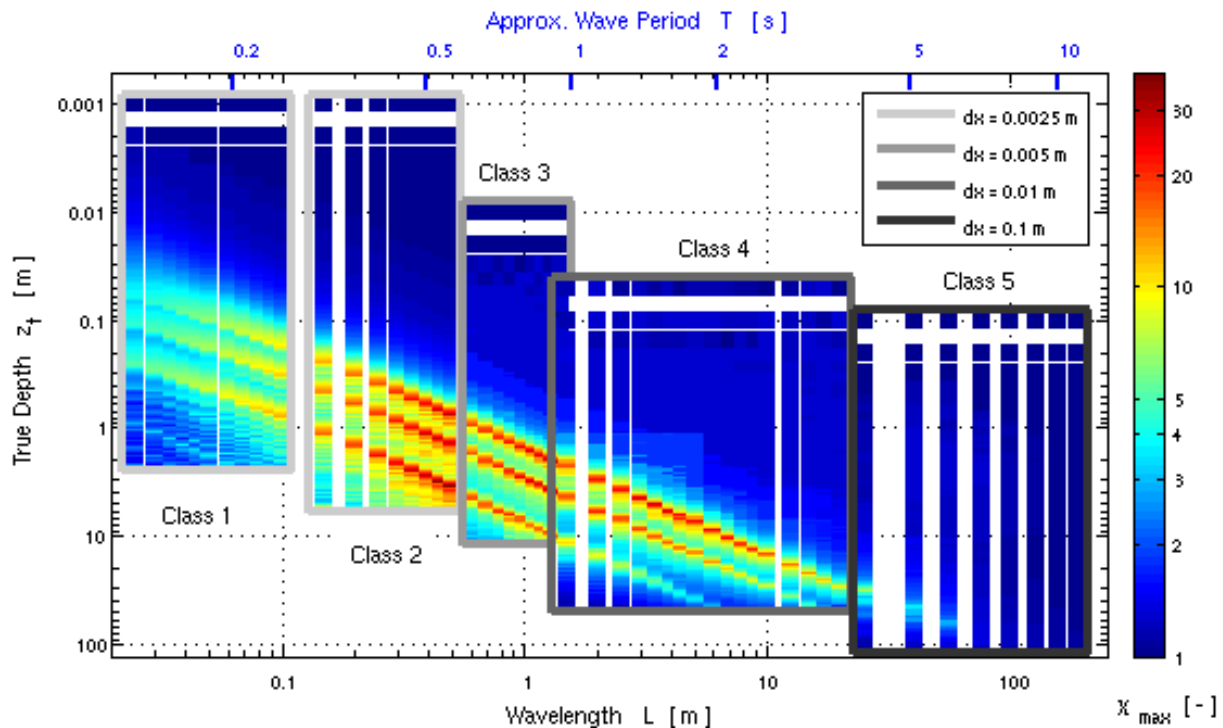


Fig. 4. Maximum possible normalized downwelling irradiance χ_{\max} due to single waves per water depth z_t and in accordance with the surface wavelength L (and period T at the top); the five framed wave classes refer to different detector sizes dx (note the logarithmic color scale).

3.2 Downwelling irradiance fields below single waves

Water waves do not represent perfect lenses and therefore do not form perfect focal points. There is always some degree of distortion or spherical aberration introduced by the wave, which is further amplified by the nonlinear wave shape. Sub-surface E_{dxz} distributions subject to about 300 regular single waves with sizes between 2.5 cm and 200 m were analyzed. The essence of all single wave simulations is assembled in Fig. 4. The color mapping indicates the maximum normalized downwelling irradiance χ_{\max} that is possible at the given wavelengths and at the three wave steepnesses under consideration. The wave period T corresponds to the light fluctuation period according to Eq. (2). The wave classes 1 to 5 are framed to underline the changing detector sizes dx . Three diagonal lines of irradiance enhancement are clearly visible. They correspond to the focal points at the particular wavelengths where the upper line corresponds to the steepest waves with $H/L = 0.09$, the middle line stands for 0.06, and the lower line for flat waves with 0.03. Remember that most wind waves have a steepness between 0.03 and 0.06. Especially at class 1, regular waves can build up deeper-lying focal points of higher order caused by neighboring waves. Their irradiance enhancements are also visible but less well pronounced. The figure basically shows the range of impact for certain waves types. For example, the

most intense light fluctuations at 1 m depth (with E_d maxima of more than 500 %) mainly arise from waves with lengths of 10 cm to 1 m (ultra-gravity waves), whereas at 10 m depth waves of 1 to 10 m length cause strongest fluctuations (ordinary gravity waves). For the first three wave classes flatter waves develop more intensive and deeper irradiance pulses at a given wavelength. Capillary waves ($L < 1.73$ cm) can produce light flashes close to the surface, but they do not directly cause the most intense light fluctuations (also observed by Stramski and Dera, 1988). The strength of enhancements at the focal points clearly decreases at the left hand side of the figure. More relevant are the well pronounced narrow light rays that follow from such very small waves. Those rays are clustered somewhat deeper due to longer waves see Fig. 5a. It becomes obvious that the longer the wave is the deeper is its potential impact. Even 200 m long swell waves can theoretically develop an enhancement of 15 % below 90 m of water depth; the coefficient of variation CV can be up to 6 %. We suggest that this E_d variability could be of ecological significance, especially in the deep light limited zone. Note that only selected wavelengths are studied. The white vertical stripes represent information gaps at wavelengths in between.

Dera and Gordon (1968) presented a sine-wave-based approximation of the focal length, which gives good agreement for flat waves with $H/L = 0.03$ up to wavelengths of 5 m.

At steeper waves nonlinearity effects of the shape become noticeable; the focal length is estimated to be considerably deeper. On the basis of our simulations for single waves, the water depth z_f of maximum radiative enhancement χ_{\max} fits to following parameterization:

$$z_f = \left[1600(H/L)^2 - 274(H/L) + 13 \right] L, \quad (9)$$

which is valid for depths down to approximately 30 m for all wave steepnesses (wavelength L ranges from 0.1 m to 5, 15, and 25 m for $H/L = 0.03$, 0.06, and 0.09, respectively). Larger waves do not necessarily accumulate most radiation within the focal point, since light beams are attenuated and scattered with increasing depth. Thus, the depth of maximum enhancement shifts upwards to the surface.

The magnitude of an irradiance pulse depends on the detector size dx and the sampling rate, e.g. a 10 cm wide sensor below a 10 cm long wave cannot resolve any enhancement; it only measures the mean value at that depth. For the present study we make use of four different horizontal grid sizes dx which basically depend on the deployment depth, or rather reflect the extent of radiometer integration time. The effects of the sensor diameter on irradiance measurements and depth resolution requirements for optical profiling are discussed by Darecki et al. (2011) and Zibordi et al. (2004). Maximum possible radiative enhancements are associated with the steepest waves ($H/L = 0.09$); nevertheless, flatter waves are much more likely. An irradiance pulse can theoretically exceed the mean irradiance by a factor of 40 at a water depth of 1 m with respect to a 2.5 mm sensor. The corresponding wave that causes the light pulse is 80 cm long. The greatest possible depth of light flashes ($\chi = 1.5$) is at approximately 80 m, and this is caused by a more than 60 m long gravity wave ($T = 6$ s, $H = 5.5$ m, and thus extremely rare occurrence probability).

Certainly, these data result from perfect laboratory waves. Superposition effects of different sized waves are important, since the overlaying restricts the ability of waves to form such efficient lensing systems. Nevertheless, near the surface comparable extreme values have been measured (Gernez et al., 2011; Darecki et al., 2011).

3.3 Light fields below irregular waves

Distributions of downwelling irradiance below irregular wave profiles are shown in Fig. 5. The light fields were simulated using three model domains with different resolutions. First, we discuss the high-resolution ray tracing model with 2.5 mm detector size that covers an area of approximately 20 m \times 5 m to study near surface fluctuations (Fig. 5a and b). Figure 5c refers to a model domain of 150 m \times 40 m with 1 cm resolution (based on the superposition of MC calculated single beam light fields). The third MC-based model covers an area of 400 m horizontal extent and 100 m depth with $dx = 10$ cm (Fig. 5d). The color coding in the figure is

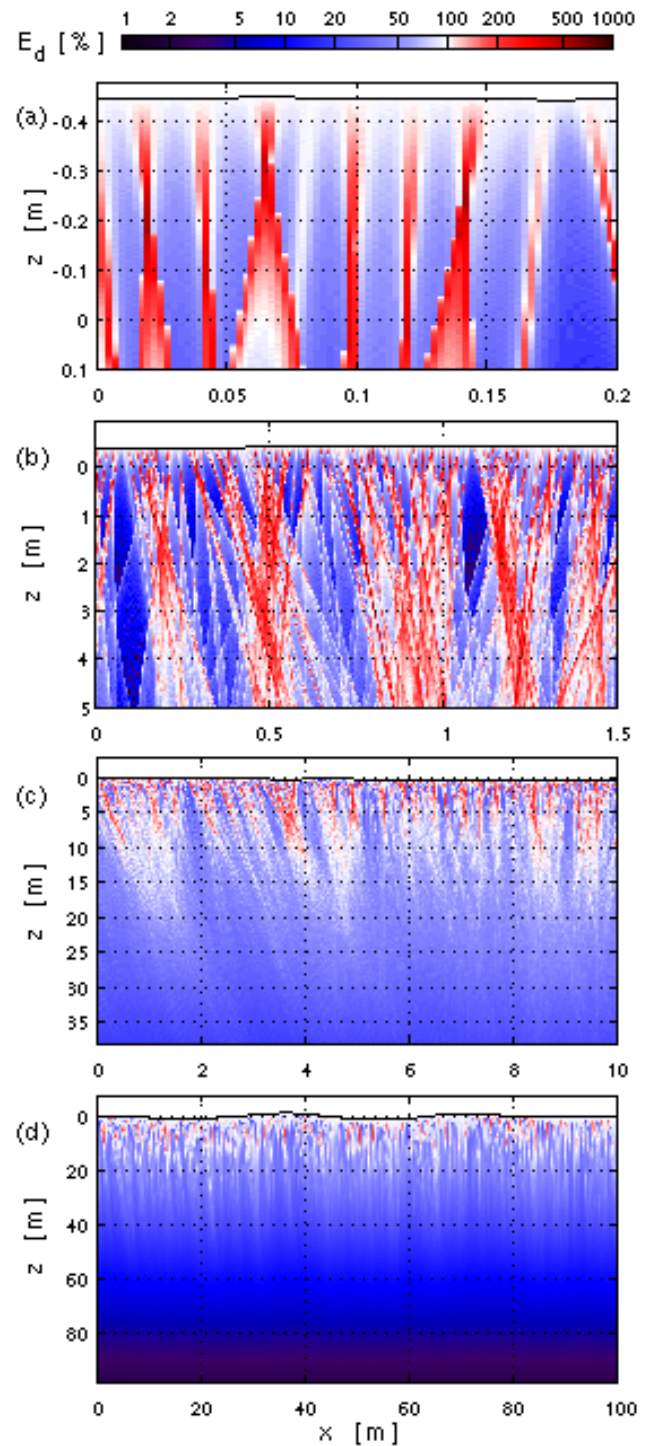


Fig. 5. Downwelling irradiance distributions beneath an irregular wave profile according to the conditions on 30 October 2009; (a) and (b) details from the near-surface model with $dx = 2.5$ mm resolution; (c) $dx = 1$ cm; (d) model resolution 10 cm (logarithmic color scale).

logarithmic again with red colors for $E_d > 100\%$ and bluish for decreasing values.

With regards to the fine structure of the sea surface, local wind in particular affects the height and thus steepness of gravity-capillary waves. The wave spectrum has a high-frequency peak at 1.7 cm wavelength and it features a clear saturation of the curvature spectrum for high wind speeds (Elfouhaily et al., 1997). Those gravity-capillary waves build up clear single stripes of E_d enhancements shown in red with focal points in depths between 10 and 50 cm (Fig. 5a). Overlaying medium-size ultra-gravity waves (Table 3), which are already much less dependent on the wind speed (Jähne and Riemer, 1990), further deflect these single rays. This leads to intensified light beam grouping at true depths of 1 to 4 m (Fig. 5b). Together with the occurrence of secondary and further focal points that are caused by neighboring gravity-capillary waves, those larger waves are responsible for very intense fluctuations and extreme irradiance peaks within the top 5 m layer. With increasing depth the gravity-capillary wave influence wears away (Fig. 5c and d); the pronounced enhancement stripes are geometrically scattered, beam focusing is reduced, and in addition the light intensity is attenuated. Image analysis of spatial underwater light fields confirms the increasing blurring of small-scale structures (Hieronymi and Macke, 2010). Under the assumption that capillary and gravity-capillary waves of 0.7 to 3 cm length are most dependent on wind friction velocity (Jähne and Riemer, 1990) we deduce that the influence of local wind on E_d fluctuations is restricted approximately to the upper 10 m of the water column. Below this layer, light variability is obviously driven by longer and thus more developed waves. During our offshore measurements, we had mainly swell dominant sea states (in terms of the relative ratio of energy associated to each wave system), which is in accordance with the relevant wave climatology (Hogben and Lumb, 1967; Sterl and Cairns, 2005). This is an interesting point since the appearance of swells may imply strong sea surface deflections, even in the absence of local wind. However, since the small-scale geometric roughness of the sea surface efficiently scatters light, the potential lensing effect of larger waves is reduced too. Generally, the wind-roughened surface affects the mean state of the light regime within the whole lit water column, which is taken into account in most radiative transfer models as for example in *HydroLight* (Mobley, 1994).

The depth-dependence of χ is illustrated in Fig. 6, where the corresponding wave profile is additionally marked (note: depth z and the wave amplitude ζ are positive downward). The top panel (Fig. 6a) shows the irradiance variability at 1 m water depth. The run of the curve is similar to observed irradiance time records as for example reported by Dera and Stramski (1986) or You et al. (2010). The irradiance variability is high and extreme irradiance pulses can exceed the mean irradiance by a factor of 8. The direct attribution of the wave shape is not distinguishable in this case. The second panel (Fig. 6b) shows χ at 20 m. Here \bar{E}_d is decreased to

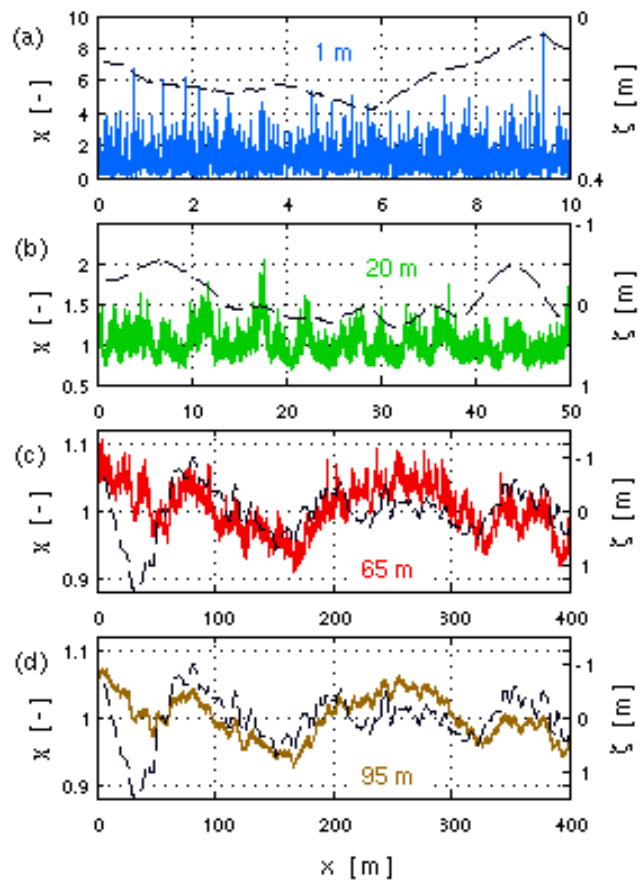


Fig. 6. Normalized downwelling irradiance χ at four different water depths with (a) 2.5 mm, (b) 1 cm, and (c) and (d) 10 cm horizontal grid resolution; on the right ordinate (dashed) is the corresponding surface elevation (30 October 2009).

about 50 % of the initial surface value; but occasionally, irradiance peaks can reach 100 % (enhancement factor $\chi = 2$). The distances between light flashes ($\chi = 1.5$) are between 2 and 10 m. With Eq. (2) this corresponds to dominant light fluctuation periods of 1.1 to 2.5 s. This again is consistent with observations at this depth and at the same wind speed (of 11 m s^{-1}) (Hieronymi and Macke, 2010). The corresponding wave structure in Fig. 6b is not clearly mirrored in the radiative profile at that depth. Deep chlorophyll maxima are often observed at depths of 65 m and more (Furuya, 1990). Figure 6c shows that here intensity peaks and also irradiance minima differ by only 10 % from the mean (E_d varies between 7.8 and 9.7 %), and that radiative fluctuations evidently reflect the large-scale surface structure. In 95 m (Fig. 6d) the χ -profile is even more smoothed on the small scale and adapted to the long gravity waves. However, the impact of fully developed ocean waves is evident.

Figure 7 shows the associated spectral information of the χ -profiles from Fig. 6. The power spectral density of light fluctuations is computed using fast *Fourier* transformation.

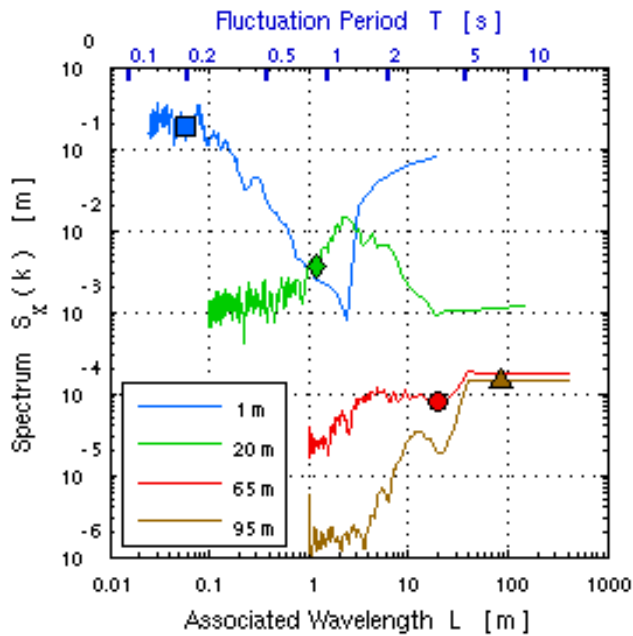


Fig. 7. Power spectral density of the four normalized irradiance profiles from Fig. 6; the mean fluctuation lengths L_m are additionally marked (30 October 2009).

The spectra show the characteristic range of corresponding water wavelengths and periods. The different magnitudes of the spectra in Fig. 7 show the strength of variance at a certain waveband that in total decreases with depth, i.e. the fluctuation amplitudes are very small at 95 m depth compared to depths near the surface. The maxima of the spectra indicate the predominant distance between two subsequent E_d peaks, e.g. the mean peak wavelength L_p at 20 m depth is 2.4 m, which corresponds to an average fluctuation period of 1.25 s. In Fig. 7, the mean fluctuation lengths L_m are additionally marked. This is the spectral center of gravity, which indicates the average wavelength (distance) of all fluctuations. In general, mean fluctuation length and period increase with increasing depth. Within the top 5 m, ultra-gravity waves dominate the light fluctuations. At 100 m depth, fluctuations have adapted to the low-frequency part of the sea spectrum, which complies with swell waves in the given example. The increasing adaptation of light fluctuation periodicity with water depth to the dominant wave of a sea state was also observed within the top 20 m by Nikolayev and Yakubenko (1978a), Fraser et al. (1980), and Wijesekera et al. (2005).

Statistical evaluations of the light field simulations are summarized in Fig. 8. The probability density functions *PDF* show similar features as records by You et al. (2010) or Gernez et al. (2011) but with much higher depth discretization ($dz = 1$ cm, 5 cm, and 10 cm). In the high-resolution model (Fig. 8 top) the fluctuation maximum is located between 25 cm and 1 m depth, which must be associated with waves of 4 cm to 1 m length (ultra-gravity waves). With

$dx = 1$ cm, the *PDF* maximum is at a depth of approximately 1 m, while in the model with $dx = 10$ cm the fluctuation maximum occurs near 5 m. Thus, the approximation of the fluctuation maximum depends on the spatial or temporal resolution. The general trend of the probability functions of all model sizes is plausible: initially the fluctuation amplitudes characteristically increase, then decrease gradually with depth (Snyder and Dera, 1970), and in the same way the level-mean irradiance decreases exponentially. Obviously, the correct choice of model size and resolution depends on the depth of interest. Near the surface irradiance fluctuations must be recorded with a high spatial resolution of $dx = 2.5$ mm and a correspondingly high temporal resolution. The model with detector width of 1 cm provides reasonable information down to about 30 m. For depths of interest beyond 20 m the 10 cm model resolution is sufficient.

The occurrence of radiative enhancements is quantified by means of a threshold analysis of the normalized downwelling irradiance profiles (Dera and Stramski, 1986; You et al., 2010). By counting the number of fluctuation amplitudes that exceed the various flash threshold levels χ_{th} , we obtain the frequency of flashes N (normalized per 1 m, and 100 m, respectively) that exceed the threshold (Fig. 8 second from left). In the upper panel, the largest χ of more than 10 can be found in 50 cm depth, which is associated with 2 to 5 cm long waves. A reason for the comparably moderate χ_{max} is the presence of strong wind (11 m s^{-1}), which impairs the efficiency of generating lens-surfaces for intense focusing. In general, the strongest near-surface fluctuations appear at relatively low wind of less than 6 m s^{-1} (Dera and Stramski, 1986; Gernez and Antoine, 2009), and χ can be larger than 13 (Gernez et al., 2011). According to the simulations with “perfect” single waves, the theoretical χ_{max} lies in the order of approximately 20 at 50 cm depth. In the same manner as the *PDF*, the flash occurrence distributions increase rapidly within the first 50 cm and then they slowly decrease. Our model with $dx = 10$ cm spatial resolution shows light flashes of $\chi = 1.5$ even down to 35 m water depth, which is much deeper than so far observed with temporal irradiance measurements. In the particular case the occurrence of light flashes at this depth range is directly associated with the sea state parameters, namely the superposition of around 40 m long waves (from the wind sea) with the 140 m swell, and it is independent of the local wind situation.

The depth-development of the coefficient of variation *CV* is shown in the panels Fig. 8 second from right. The fundamental curve progression and the orders of magnitudes of *CV*, which depend on the resolution, correspond to previous observations (e.g. Nikolayev and Khulapov, 1976; Gernez and Antoine, 2009; Hieronimi and Macke, 2010; D’Alimonte et al., 2010; Weber, 2010). The figure shows that underwater light field fluctuations occur even in 100 m depth, where (with the specified irregular wave profile) *CV* is still about 3%. However, wave-induced light fluctuations depend on local wind and the peculiarity of the sea state. According

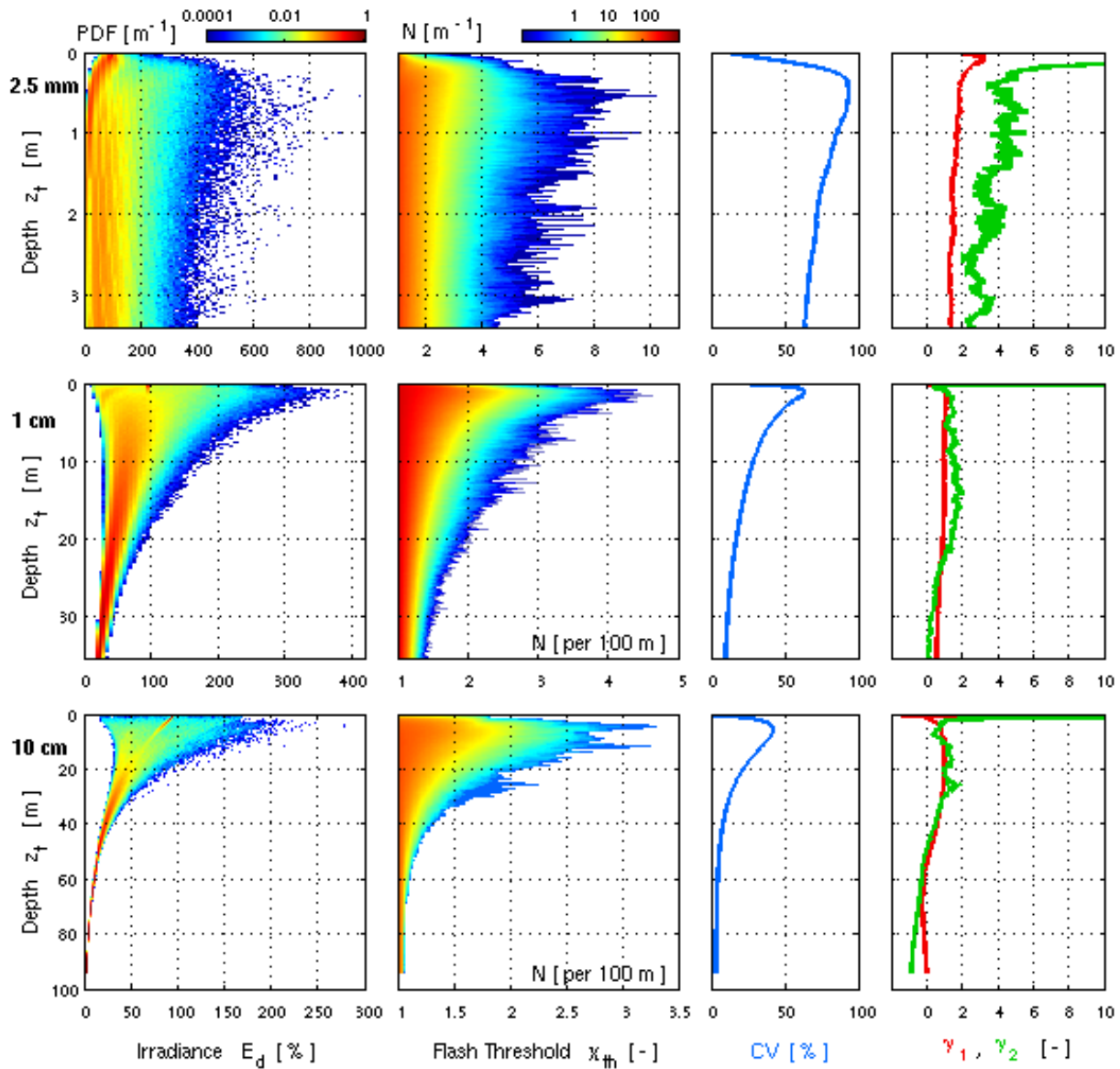


Fig. 8. Statistical evaluation of the modeled light field for 30 October 2009; top: near the surface with 2.5 mm resolution, middle row: $dx = 1$ cm, and lower panels: $dx = 10$ cm; each shown the probability density function PDF , frequency of flashes N above a certain threshold x_{th} , coefficient of variation CV , and PDF skewness γ_1 , and excess kurtosis γ_2 .

to a theoretical study by Weber (2010), CV exhibits a bimodal dependence on the depth, with a near-surface CV maximum that shifts towards smaller depths with increasing wind velocity, a local CV minimum, which is around a depth of 300 m in clear oceanic water, and a second maximum, which is located at “fairly large optical depths” (investigations down to 10^5 m water depth). Our model considers depths to 100 m only; here the remaining irradiance is small and the fraction of unscattered light is less than 0.1 % compared to the total downwelling irradiance with the given input parameters. Figure 4 documents the dwindling ability all wave types to focus light within the top 100 m. Thus, the wave-influence on

the subsurface light field, and especially CV , beyond 300 m water depth cannot be confirmed with our work. The unique influence of local wind and especially the development of the sea state have to be subject to further analysis.

The skewness γ_1 and excess kurtosis γ_2 of the PDF s are shown on the right side of Fig. 8. The skewness of the irradiance distribution is a measure for the deflection direction of extreme intensity peaks. Above 54 m the E_d distributions are right-skewed, i.e. more intense radiative enhancements appear than E_d reductions. Below that depth the distribution is slightly negatively skewed. The excess kurtosis is a measure for the peakedness of the irradiance distribution

compared to a *Gaussian* distribution (kurtosis minus 3). Positive excess kurtosis means that a larger part of the variance results from extreme intensity peaks. With increasing depth the *PDFs* become more grouped around the mean value. In principle, all model sizes deliver equivalent results. Slight deviations result from the different resolutions. Generally, the depth-dependency of our simulated *PDF* skewness and excess kurtosis fits to high-frequency irradiance measurements by Gernez et al. (2011). They show that close to the surface (<1 m), these parameters can assume values larger than 3 and 20, respectively (the same maximum values in our case), and that both are reduced to nearly zero at 10 m depth (they refer to 532 nm wavelength and more turbid water). In addition, they suggest that the skewness and excess kurtosis of the downwelling irradiance *PDF* could be used to partition the oceanic photonic zone into the sunny and diffuse layer, expressions that are introduced by Dera (1970) to essentially differentiate the areas with and without light flashes. According to this, the depth of the sunny layer bottom is where both, γ_1 and γ_2 , approach zero. In our simulations with $dx = 10$ cm, the skewness and the excess kurtosis approach zero at about 50 m. The precision of our statistical results could be increased by considering a light field of more than 400 m width (from a 500 m wave profile) and thus more regarding the impacts on the *PDF* (especially in greater water depths) of swell waves, which are 140 m long in the considered case (swell period 9.5 s). Our model provides comprehensible and logical statistical results down to 100 m depth and furthermore, it is the first model that gives such high-resolution information on wave-induced light field fluctuations.

4 Conclusions

We developed a novel radiative transfer model for simulating light field fluctuations (that are caused by surface waves) down the water column. The spatial propagation of solar radiation in water, i.e. the light scattering and absorption, is calculated by means of a special Monte Carlo radiative transfer procedure. The model is generally adaptive for several variables, such as the electromagnetic wavelength, inherent optical properties of seawater, different lighting conditions, different light field resolutions, and above all for arbitrary sea surface structures, for which the model is optimized. The resulting underwater light fields, which are quantified by the distribution of the downwelling irradiance, cover large 2-D domains with comparable high spatial resolution (2.5 mm to 10 cm) and great depths (down to 100 m). Vertical deflections of irregular sea surfaces, in orders of magnitude between capillary and fully developed gravity waves, can be implemented into the model. The model is relatively fast (since the Monte Carlo procedure is decoupled from geometric ray tracing) and it provides all statistical properties of the light regime. The modeled fluctuation characteristics fit to previously pub-

lished observations, and beyond this, show a high information density into much greater depths (to 100 m). The mean values of the downwelling irradiance are within the usual error margins compared to offshore measurements and other radiometric transfer models, as e.g. *HydroLight*. Thus, the introduced radiative transfer model provides some important advantages compared to other current models (Deckert and Micheal, 2006; D'Alimonte et al., 2010; You et al., 2010).

By means of the model, underwater light variability was simulated for different single waves and for realistic wave situations in the open ocean. The latter agree well with equivalent in-situ measurements. The model parameters are selected in such a manner that maximum irradiance variability can be achieved, i.e. monochromatic light at 490 nm, very clear water, and high sun elevation are used for the calculations. Simulations have been performed for more than 300 nonlinearly shaped single waves of all sizes that appear in the open ocean. In general, the depth-impact of waves depends on their length and steepness, the longer the wave the deeper is its potential influence. We provide expectation values of maximum possible wave focusing per depth, e.g. at 1 m water depth light flashes can theoretically exceed the mean irradiance by a factor of 40 (with $dx = 2.5$ mm). The greatest theoretically possible depth of light flashes with 50 % radiative enhancement should be around 80 m (with $dx = 10$ cm), which would be caused by a very steep ($H/L = 0.09$) gravity wave over 60 m long. Even 200 m long swell waves can develop E_d fluctuations within a range of ± 15 % compared to the mean value below 90 m of water depth.

The superposition of short and long waves from the ocean wave spectrum at the water surface leads to characteristic probability distributions of downwelling irradiance in the water column. Local wind primarily affects the development and steepness of capillary and gravity-capillary waves of 0.7 to 3 cm length, with a typical high-frequency peak in the wave spectrum at 1.7 cm. The resulting irradiance maxima due to those gravity-capillary wave lenses can be found within the top 1 m near the surface. A further deflection of light beams is forced by overlaying ultra-gravity waves (less than 1 m long), which are already much less directly wind-dependent. This leads to intensified light beam grouping at 1 to 4 m depth, but certainly with decreasing frequency of the occurrence of extreme light flashes. We suggest that the influence of local wind on light fluctuations is restricted to approximately the upper 10 m of the water column. Below this layer, light variability is obviously driven by longer and thus more developed waves. With increasing water depth, light fluctuation periodicity adapts more and more to the long-wave part of the sea spectrum, i.e. to the dominant wave of the sea state.

Our model results of natural irregular light fields suggest that light flashes with 50 % irradiance enhancements can appear even in 35 m depth (with low occurrence probability). In addition, under high sea conditions light variability of less than $\bar{E}_d \pm 10$ % ($CV < 5$ %) is possible still in 100 m depth.

The modeling results have to be verified with adequate in-situ measurements at sea; our deepest measured light flash was at about 20 m depth.

Certainly, a future question is the relevance of this deep-water light variability for different photo-relevant processes. Below approximately 10 m depth, the photosynthetically active radiation *PAR* (400–700 nm) is strongly dominated by the blue-green spectral components and the used 490 nm can be considered representative for this waveband. Thus, we suggest that the described fluctuation characteristics at 490 nm can be a good approximation for the variability of the entire *PAR* value.

Acknowledgements. This work was supported by the German Research Foundation *DFG* (contract MA 2225/11-1) and the Kiel Cluster of Excellence “*The Future Ocean*”. We express our gratitude to Curtis D. Mobley for making the *HydroLight* software available. Model comparative measurements have been carried out in the framework of the *OCEANET* project on board the R/V *Polarstern*, cruise ANT-XXVI/1; the assistance of the crew and members of the working group is highly appreciated. Finally, we thank the editor John M. Huthnance and the anonymous reviewers for suggestions that improved the paper.

Edited by: J. M. Huthnance

References

- Babanin, A. V.: On a wave-induced turbulence and a wave-mixed upper ocean layer, *Geophys. Res. Lett.*, 33, L20605, doi:10.1029/2006GL027308, 2006.
- Cox, C. and Munk, W.: Measurements of the roughness of the sea surface from photographs of the sun’s glitter, *J. Opt. Society Am.*, 44, 838–850, 1954.
- Cullen, J. J.: The deep chlorophyll maximum: comparing vertical profiles of chlorophyll a, *Can. J. Fish. Aquat. Sci.*, 39, 791–803, doi:10.1139/f82-108, 1982.
- D’Alimonte, D., Zibordi, G., Kajiyama, T., and Cunha, J. C.: Monte Carlo code for high spatial resolution ocean color estimation, *Appl. Opt.*, 49, 4936–4950, doi:10.1364/AO.49.004936, 2010.
- Darecki, M., Stramski, D., and Sokolski, M.: Measurements of high-frequency light fluctuations induced by ocean surface waves with an underwater porcupine radiometer system, *J. Geophys. Res.*, 116, C00H09, doi:10.1029/2011JC007338, 2011.
- de Boyer Montegut, C., Madec, G., Fischer, A. S., Lazar, A., and Iudicone, D.: Mixed layer depth over the global ocean: An examination of profile data and a profile-based climatology, *J. Geophys. Res.*, 109, C12003, doi:10.1029/2004JC002378, 2004.
- Deckert, R. and Michael, K. J.: Lensing effect on underwater levels of UV radiation, *J. Geophys. Res.*, 111, C05014, doi:10.1029/2005JC003332, 2006.
- Dera, J.: On two layers of different light conditions in the euphotic zone in the sea, *Acta Geophys. Pol.*, 18, 287–294, 1970.
- Dera, J. and Gordon, H. R.: Light field fluctuations in the photic zone, *Limnol. Oceanogr.*, 13, 697–699, 1968.
- Dera, J. and Stramski, D.: Maximum effects of sunlight focusing under a wind-disturbed sea surface, *Oceanologia*, 23, 15–42, 1986.
- Dickey, T., Granata, T., Marra, J., Langdon, C., Wiggert, J., Chai-Jochner, Z., Hamilton, M., Vazquez, J., Stramska, M., Bidigare, R., and Siegel, D.: Seasonal variability of bio-optical and physical properties in the Sargasso Sea, *J. Geophys. Res.*, 98, 865–898, doi:10.1029/92JC01830, 1993.
- Dickey, T. D., Kattawar, G. W., and Voss, K. J.: Shedding new light on light in the ocean, *Phys. Today*, 64, 44–49, doi:10.1063/1.3580492, 2011.
- Elfouhaily, T., Chapron, B., Katsaros, K., and Vandemark, D.: A unified directional spectrum for long and short wind-driven waves, *J. Geophys. Res.*, 102, 15781–15796, doi:10.1029/97JC00467, 1997.
- El Naggar, S. and Macke, A. (Ed.): The expedition of the Research Vessel “Polarstern” to the Antarctic in 2009 (ANT-XXVI/1), Reports on Polar and Marine Research, 614, 79 pp., doi:10013/epic.35280, 2010.
- Falkowski, P. G.: Physiological responses of phytoplankton to natural light regimes, *J. Plankton Res.*, 6, 295–307, doi:10.1093/plankt/6.2.295, 1984.
- Fell, F. and Fischer, J.: Numerical simulation of the light field in the atmosphere-ocean system using the matrix-operator method, *J. Quant. Spectrosc. Ra.*, 69, 351–388, doi:10.1016/S0022-4073(00)00089-3, 2001.
- Fraser, A. B., Walker, R. E., and Jurgens, F. C.: Spatial and temporal correlation of underwater sunlight fluctuations in the Sea, *IEEE J. Oceanic Eng.*, 5, 195–198, doi:10.1109/JOE.1980.1145467, 1980.
- Furuya, K.: Subsurface chlorophyll maximum in the tropical and subtropical western Pacific Ocean: vertical profiles of phytoplankton biomass and its relationship with chlorophyll a and particulate organic carbon, *Mar. Biol.*, 107, 529–539, doi:10.1007/BF01313438, 1990.
- Gernez, P. and Antoine, D.: Field characterization of wave-induced underwater light field fluctuations, *J. Geophys. Res.*, 114, C06025, doi:10.1029/2008JC005059, 2009.
- Gernez, P., Stramski, D., and Darecki, M.: Vertical changes in the probability distribution of downwelling irradiance within the near-surface ocean under clear sky conditions, *J. Geophys. Res.*, 116, C00H07, doi:10.1029/2011JC007156, 2011.
- Gordon, H. R. and Morel, A.: Remote assessment of ocean color for interpretation of satellite visible imagery, A review, in: *Lecture Notes on Coastal and Estuarine Studies*, edited by: Barber, R. T., Mooers, C. N. K., Bowman, M. J., and Zeitzchel, B., Springer, New York, 114 pp., 1983.
- Hieronimi, M.: Solar radiative transfer into the ocean: A study on underwater light fluctuations due to surface waves, Ph.D. thesis, Christian-Albrechts-Universität zu Kiel, Germany, 103 pp., 2011.
- Hieronimi, M. and Macke, A.: Spatiotemporal underwater light field fluctuations in the open ocean, *J. Europ. Opt. Soc. Rap. Public.*, 5, 1–8, 10019S, doi:10.2971/JEOS.2010.10019S, 2010.
- Hogben, N. and Lumb, F. E.: *Ocean wave statistics*, HMSO, London, 1967.
- Jähne, B. and Riemer, K. S.: Two-dimensional wave number spectra of small-scale water surface waves, *J. Geophys. Res.*, 95, 11531–11546, doi:10.1029/JC095iC07p11531, 1990.
- Kantha, L.: A note on the decay rate of swell, *Ocean Modell.*, 11, 167–173, doi:10.1016/j.ocemod.2004.12.003, 2006.
- Kinsman, B.: *Wind Waves: their generation and propagation on the*

- ocean surface, Englewood Cliffs, N. J., Prentice-Hall, 1965.
- Kirk, J. T. O.: Monte Carlo study of the nature of the underwater light field in, and the relationship between optical properties of, turbid yellow water, *Aust. J. Mar. Freshwater Res.*, 32, 517–532, doi:10.1071/MF9810517, 1981.
- Longuet-Higgins, M. S.: The effect of non-linearities on statistical distributions in the theory of sea waves, *J. Fluid Mech.*, 17, 459–480, doi:10.1017/S0022112063001452, 1963.
- Longuet-Higgins, M. S.: On the skewness of sea-surface slopes, *J. Phys. Oceanogr.*, 12, 1283–1291, doi:10.1175/1520-0485(1982)012<1283:OTSOSS>2.0.CO;2, 1982.
- Macke, A.: Monte Carlo calculations of light scattering by large particles with multiple internal inclusions, in: *Light scattering by nonspherical particles: Theory, measurements, and applications*, edited by: Mishchenko, M. I., Hovenier, J. W., and Travis, L. D., San Diego, Academic Press, 309–322, 2000.
- Marcos, M., Seymour, J. R., Luhar, M., Durham, W. M., Mitchell, J. G., Macke, A., and Stocker, R.: Microbial alignment in flow changes ocean light climate, *P. Natl. Acad. Sci. USA*, 108, 10, 3860–3864, doi:10.1073/PNAS.1014576108, 2011.
- Mobley, C. D.: *Light and water: Radiative transfer in natural waters*, San Diego, Academic Press, 592 pp., 1994.
- Mobley, C. D., Gentili, B., Gordon, H. R., Jin, Z., Kattawar, G. W., Morel, A., Reinersman, P., Stamnes, K., and Stavn, R. H.: Comparison of numerical models for computing underwater light fields, *Appl. Opt.*, 32, 7484–7504, doi:10.1364/AO.32.007484, 1993.
- Morel, A.: Optical modeling of the upper ocean in relation to its biogenous matter content (Case I waters), *J. Geophys. Res.*, 93, 10749–10768, doi:10.1029/JC093iC09p10749, 1988.
- Morel, A.: Are the empirical relationships describing the bio-optical properties of case I waters consistent and internally compatible?, *J. Geophys. Res.*, 114, C01016, doi:10.1029/2008JC004803, 2009.
- Morel, A. and Gentili, B.: Diffuse reflectance of oceanic waters: its dependence on sun angle as influenced by the molecular scattering contribution, *Appl. Opt.*, 30, 4427–4438, doi:10.1364/AO.30.004427, 1991.
- Morel, A. and Prieur, L.: Analysis of variations in ocean color, *Limnol. Oceanogr.*, 22, 709–722, 1977.
- Morel, A., Antoine, D., and Gentili, B.: Bidirectional reflectance of oceanic waters: accounting for Raman emission and varying particle scattering phase function, *Appl. Opt.*, 41, 6289–6306, doi:10.1364/AO.41.006289, 2002.
- Morel, A., Gentili, B., Claustre, H., Babin, M., Bricaud, A., Ras, J., and Tieche, F.: Optical properties of the “clearest” natural waters, *Limnol. Oceanogr.*, 52, 217–229, doi:10.4319/LO.2007.52.1.0217, 2007.
- Nikolayev, V. P. and Khulapov, M. S.: Use of a nonstatistical model to explain the mechanism of underwater illumination fluctuations, *Izv. Atmospheric and Oceanic Physics*, 12, 993–997, 1976.
- Nikolayev, V. P. and Prokopov, O. I.: The relationship between the statistical characteristics of underwater illumination and certain lighting conditions of the sea surface, *Izv. Atmospheric and Oceanic Physics*, 13, 734–738, 1977.
- Nikolayev, V. P. and Yakubenko, V. G.: On the relationship between the statistical characteristics of the underwater light field and the wave state characteristics, *Izv. Atmospheric and Oceanic Physics*, 14, 88–92, 1978a.
- Nikolayev, V. P. and Yakubenko, V. G.: Experimental research into the spatial structure of the fluctuations of the underwater light field, *Izv. Atmospheric and Oceanic Physics*, 14, 301–305, 1978b.
- Nikolayev, V. P., Prokopov, O. I., Rozenberg, G. V., and Shevernev, V. I.: Statistical properties of the underwater illumination, *Izv. Atmospheric and Oceanic Physics*, 8, 936–944, 1972.
- Ochi, M. K. and Hubble, E. N.: Six-parameter wave spectra, *Proc. 15th Coastal Engineering Conf.*, 301–328, 1976.
- Petzold, T. J.: Volume scattering functions for selected ocean waters, Scripps Institution of Oceanography, San Diego, Ref. 72–78, 1972.
- Plass, G. N. and Kattawar, G. W.: Monte Carlo calculations of radiative transfer in the Earth’s atmosphere-ocean system: 1. Flux in the atmosphere and ocean, *J. Phys. Oceanogr.*, 2, 139–145, doi:10.1175/1520-0485(1972)002<0139:MCCORT>2.0.CO;2, 1972.
- Plass, G. N., Kattawar, G. W., and Guinn Jr., J. A.: Radiative transfer in the earth’s atmosphere and ocean: influence of ocean waves, *Appl. Opt.*, 14, 1924–1936, doi:10.1364/AO.14.001924, 1975.
- Pope, R. M. and Fry, E. S.: Absorption spectrum (380–700 nm) of pure water. II. Integrating cavity measurements, *Appl. Opt.*, 36, 8710–8723, doi:10.1364/AO.36.008710, 1997.
- Preisendorfer, R. W. and Mobley, C. D.: Albedos and glitter patterns of a wind-roughened sea surface, *J. Phys. Oceanogr.*, 16, 1293–1316, doi:10.1175/1520-0485(1986)016<1293:AAGPOA>2.0.CO;2, 1986.
- Schenck Jr., H.: On the focusing of sunlight by ocean waves, *J. Opt. Soc. Am.*, 47, 653–657, doi:10.1364/JOSA.47.000653, 1957.
- Segelstein, D. J.: The complex refractive index of water, MS thesis, University of Missouri, Kansas City, 1981.
- Snyder, R. L. and Dera, J.: Wave-induced light field fluctuations in the Sea, *J. Opt. Soc. Am.*, 60, 1072–1079, doi:10.1364/JOSA.60.001072, 1970.
- Sterl, A. and Caires, S.: Climatology, variability and extrema of ocean waves: The web-based NKMI/ERA-40 wave atlas, *Int. J. Climatol.*, 25, 963–977, doi:10.1002/JOC.1175, 2005.
- Stramski, D. and Dera, J.: On the mechanism for producing flashing light under a wind-disturbed water surface, *Oceanologia*, 25, 5–21, 1988.
- Stramski, D. and Tegowski, J.: Effects of intermittent entrainment of air bubbles by breaking wind waves on ocean reflectance and underwater light field, *J. Geophys. Res.*, 106, 31345–31360, doi:10.1029/2000JC000461, 2001.
- Walker, R. E.: *Marine light field statistics*, Wiley Series in Pure and Applied Optics, p. 675, ISBN 0471310468, 1994.
- Walsh, P. and Legendre, L.: Photosynthesis of natural phytoplankton under high frequency light fluctuations simulating those induced by sea surface waves, *Limnol. Oceanogr.*, 28, 688–697, 1983.
- Wang, M., Knobelspiesse, K. D., and McClain, C. R.: Study of the Sea-Viewing Wide Field-of-View Sensor (SeaWiFS) aerosol optical property data over ocean in combination with the ocean color products, *J. Geophys. Res.*, 110, D10S06, doi:10.1029/2004JD004950, 2005.
- Weber, V. L.: Coefficient of variation of underwater irradiance fluctuations, *Radiophysics and Quantum Electronics*, 53, 13–27, 2010.

- Wijesekera, H. W., Pegau, W. S., and Boyd, T. J.: Effects of surface waves on the irradiance distribution in the upper ocean, *Opt. Express*, 13, 9257–9264, doi:10.1364/OPEX.13.009257, 2005.
- Wozniak, B., Dera, J., Ficek, D., Majchrowski, R., Ostrowska, M., and Kaczmarek, S.: Modelling light and photosynthesis in the marine environment, *Oceanologia*, 45, 171–245, 2003.
- Yakubenko, V. G. and Nikolayev, V. P.: Numerical modeling of the fluctuations of the light field beneath a rough sea surface, *Izv. Atmospheric and Oceanic Physics*, 13, 135–139, 1997.
- You, Y., Stramski, D., Darecki, M., and Kattawar, G. W.: Modeling of wave-induced irradiance fluctuations at the near-surface depths in the ocean: a comparison with measurements, *Appl. Opt.*, 49, 1041–1053, doi:10.1364/AO.49.001041, 2010.
- Zaneveld, J. R. V., Boss, E., and Barnard, A.: Influence of surface waves on measured and modeled irradiance profiles, *Appl. Opt.*, 40, 1442–1449, doi:10.1364/AO.40.001442, 2001.
- Zhang, X., He, M. X., Yang, Q., and Zeng, K.: Effects of wind on ocean color, *IGARSS 2006*, 4056–4059, doi:10.1109/IGARSS.2006.1040, 2006.
- Zibordi, G. and Voss, K. J.: Geometrical and spectral distribution of sky radiance: Comparison between simulations and field measurements, *Remote Sens. Environ.*, 27, 343–358, doi:10.1016/0034-4257(89)90094-1, 1989.
- Zibordi, G., D’Alimonte, D., and Berthon, J. F.: An evaluation of depth resolution requirements for optical profiling in coastal waters, *J. Atmos. Ocean. Tech.*, 21, 1059–1073, 2004.
- Zielinski, O., Llinás, O., Oschlies, A., and Reuter, R.: Underwater light field and its effect on one-dimensional ecosystem model at station ESTOC, north of the Canary Islands, *Deep-Sea Res. Pt. II*, 49, 3529–3542, doi:10.1016/S0967-0645(02)00096-6, 2002.